Synthesis of few-layered, high-purity graphene oxide sheets from different graphite sources for biology

2016 2D Mater. 3 014006

(http://iopscience.iop.org/2053-1583/3/1/014006)

2D Materials

OPEN ACCESS

RECEIVED
28 September 2015

REVISED
24 November 2015

ACCEPTED FOR PUBLICATION
4 December 2015

PUBLISHED
4 February 2016

PAPER

Synthesis of few-layered, high-purity graphene oxide sheets from different graphite sources for biology

Dhifaf A Jasim, Neus Lozano and Kostas Kostarelos

Nanomedicine Laboratory, Faculty of Medical & Human Sciences and National Graphene Institute, University of Manchester, AV Hill Building, Manchester M13 9PT, UK

E-mail: kostas.kostarelos@manchester.ac.uk

Keywords: carbon, graphene, cytotoxicity, nanotoxicology, biointerface

Abstract

This work aimed to interrogate the role that the starting graphitic material played on the physicochemical properties of graphene oxide (GO) sheets and their impact on mammalian cell viability following exposure to those flakes. Three different GO thin sheets were synthesised from three starting graphite material: flakes (GO-f), ground (GO-g) and powder (GO-p) using a modified Hummers' method. The synthetic yield of this methodology was found to differ according to type of starting material, with GO-p resulting in most efficient yields. Structural and morphological comparison of the three GO sheet types were carried out using transmission electron microscopy and atomic force microscopy. Optical properties were measured using UV/visible and fluorescence spectroscopy. Surface characteristics and chemistry were determined using a battery of techniques. Exposure to human cells was studied using the human A549 lung epithelial cultures. Our results revealed that all three GO samples were composed of few-layer sheets with similar physicochemical and surface characteristics. However, significant differences were observed in terms of their lateral dimensions with GO-p, prepared from graphite powder, being the largest among the GOs. No cytotoxicity was detected for any of the GO samples following exposure onto A549 cells up to 48 h. In conclusion, the form and type of the starting graphite material is shown to be an important factor that can determine the synthetic yield and the structural characteristics of the resulting GO sheets.

Introduction

Graphene is the thinnest and strongest free standing two-dimensional (2D) crystal reported in 2004 [1, 2]. Its unique honeycomb carbon geometry gives rise to exceptional physicochemical properties that has led to intense interest from different scientific disciplines, ranging from material science, engineering and more recently biomedicine [3–6]. Graphene oxide (GO), the oxidised derivative of graphene, has been extensively surface-modified with oxygen-rich groups has been explored in many fields, due to its hydrophilic nature and colloidal stability in aqueous environments [7–9].

Graphene and its multiple types of derivatives are prepared by several methods. Bottom-up synthesis methods involve growing on substrate surfaces, such as epitaxial growth, where the carbon source is added within the substrate surface. Alternatively, in chemical vapour deposition, carbon is added in the form of a methane gas [10]. Top-down synthesis methods, like mechanical exfoliation of graphite, is another commonly used method to prepare graphene suspensions [11, 12]. Sonication of graphite in solutions also results in exfoliation into single layered graphene [13]. A third method that has been considered is the reduction of exfoliated graphite oxide by thermal or chemical means that produces reduced graphene oxide (rGO) this bears considerably less remaining oxygens and is closer to pristine graphene [14]. Recently, graphene has also been prepared by ball milling [15]. All of these exfoliation methods can give rise to high-quality and purity graphene sheets, but yet can offer no control on the dimensionality of the ensuing sheets [16–18]. Bottom-up methods have better controllability of size,

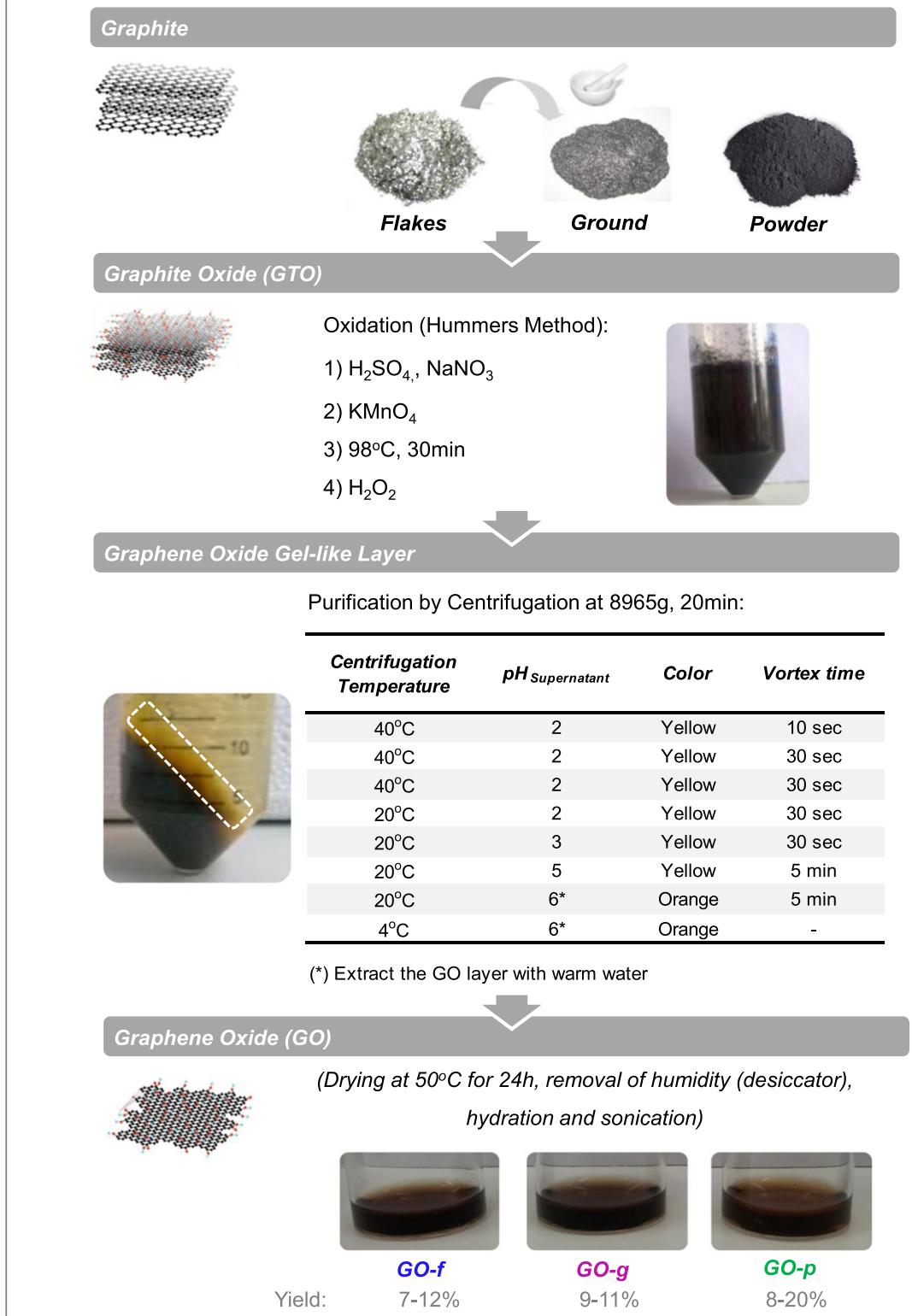

Scheme 1. Preparation of GO by a modified Hummers' method from different forms of graphite; flakes, ground and powder. Extraction of the gel-like layer in each sample allows for purification of mainly thin (single, double or few layer) GO sheets that is considered essential for biomedical applications.

thickness and even shape [10, 16]. However, the graphene material prepared by these methods contain impurities and exhibit wide variability in surface and structural characteristics, due to the multiple and random defects and grain boundaries induced [16]. Some other methods that are less popular for large scale production of graphene sheets involve unzipping or splitting carbon nanotubes by chemical or physical means [12].

Graphene oxide (GO) can also be synthesised by several methods. Staudenmaier [19, 20], Hofmann [21], Hummers [22] and Tour [23] have all described

Table 1. Yields obtained of GO prepared from different sources of graphite.

Starting graphite	GO sample	Yield in mg	% Yield from starting graphite
Flakes	GO-f	36.5 ± 10.3	9.1 ± 2.6
Ground	GO-g	38.9 ± 4.5	9.7 ± 1.1
Powder	GO-p	70.3 ± 19.3	17.6 ± 4.8

methodologies that constitute robust chemical strategies for production of GO [7]. Other synthetic strategies involve growing of monolayer and multilayer GO thin films on cationic surfaces [25]. Of all these, the Hummers method has been the most widely used method for production of GO today. Various modifications of this method have been introduced to improve the synthesis and purity of the final product [9, 24]. However, from all these methods and synthetic approaches the products are largely variable in terms of surface properties (e.g. oxidation extent/ratio of sp^2 and sp^3 domains), structural features (e.g. lateral size and thickness), purity and colloidal dispersibility. This can be due to the differences in reaction conditions, type of graphitic material [26] and purification processing used [19]. It is expected that the presence of multiple forms of graphene materials or impurities in a sample would result in significant differences on interaction with biological matter and the subsequent responses [27–31]. More importantly for graphene materials, their surface and structural characteristics will play a central role in determining its biological fate [32, 33]. There are many reports studying the interaction of pristine graphene [34–37], GO [38–41] and rGO [42, 43] with cell cultures, yet only limited and commonly contradictory information is available, making generalisations and conclusions inaccurate [4, 33]. We believe this, to a large part, is due to the wide variability among the material used, processed and the methods they are allowed to interact with cells.

In this study, we aimed to interrogate the role that the starting graphitic material may have on the resulting GO material characteristics and their impact on mammalian cell cultures. To do that, the synthetic methodology was established and different forms of graphite were used; namely, graphite flakes (f), ground graphite (g) and graphite powder (p) resulting in the production of GO-f, GO-g and GO-p, respectively. The modified Hummers method that we previously adapted to synthesise thin GO sheets of high purity [24] was used throughout this study. Extensive characterisation of the material by several techniques was carried out to determine their differences in structural, optical and surface properties. Since the lung is considered one of the main organs of unintended nanomaterial exposure, biological responses were studied on human lung epithelial (A549) cell cultures.

Results

Synthesis of graphene oxide from different graphite sources

GO samples were prepared from different graphite forms using the Hummers method modified for the purposes of producing aqueous dispersions of biological-grade sheets, as described in the Experimental section. Briefly, the GO prepared by this method critically depends on the separation of a brownish graphene oxide gel-like layer (scheme 1) that rests on top of the by-products from the oxidation reaction, along the thick graphitic and graphitic oxide (black) material [9]. The GO gel-like layer starts appearing when the pH of the supernatant is neutralised, after several centrifugation rounds. All GO samples were well-dispersed as a brownish aqueous colloidal suspension of physiological pH and stable at room temperature for more than 6 months (scheme 1). yields at the end of the complete process for the different GO are listed in table 1. The GO prepared from graphite powder (GO-p) produced consistently double the yield compared to the GO prepared either from flakes (GO-f) or ground graphite (GO-g), presumably due to the higher surface area of the powder graphite.

Structural properties and morphology

The morphology of the samples is shown in the transmission electron microscopy (TEM) and atomic force microscopy (AFM) images in figures 1(i) and (ii). GO-p, prepared from graphite powder, was the largest in terms of lateral dimension distribution, while GO-g was the smallest, followed by GO-f, as determined by AFM size measurements. All GO sheets were few layered (~1–4 nm thick; 1–5 layers), as shown by the AFM height images in figure 1. Lateral size distribution was wide, but most GO flakes were generally smaller than 1 μm for all samples as shown in figures 1(Aiii), (Biii), (Ciii).

Optical (absorbance and fluorescence) properties

GO samples prepared showed the characteristic absorbance peak around 230 nm with a shoulder around 300 nm (figures 2(A)–(C)). The inset graphs show the calibration curve at 230 nm for each corresponding GO sample. Fluorescence spectra of GO samples revealed that all samples contained two excitation wavelengths at 483 nm (data not shown) and 525 nm, with a broad emission in the visible region 550–600 nm. The maximum excitation at 525 nm was only considered since this offers more defined and linear emission peaks (figure 3(A)). GO-p had the most intense and prominent emission peak among the three GO samples. These results were also confirmed by fluorescence imaging using the IVIS camera, commonly used in biomedical imaging, shown in figures 3(B) and (C).

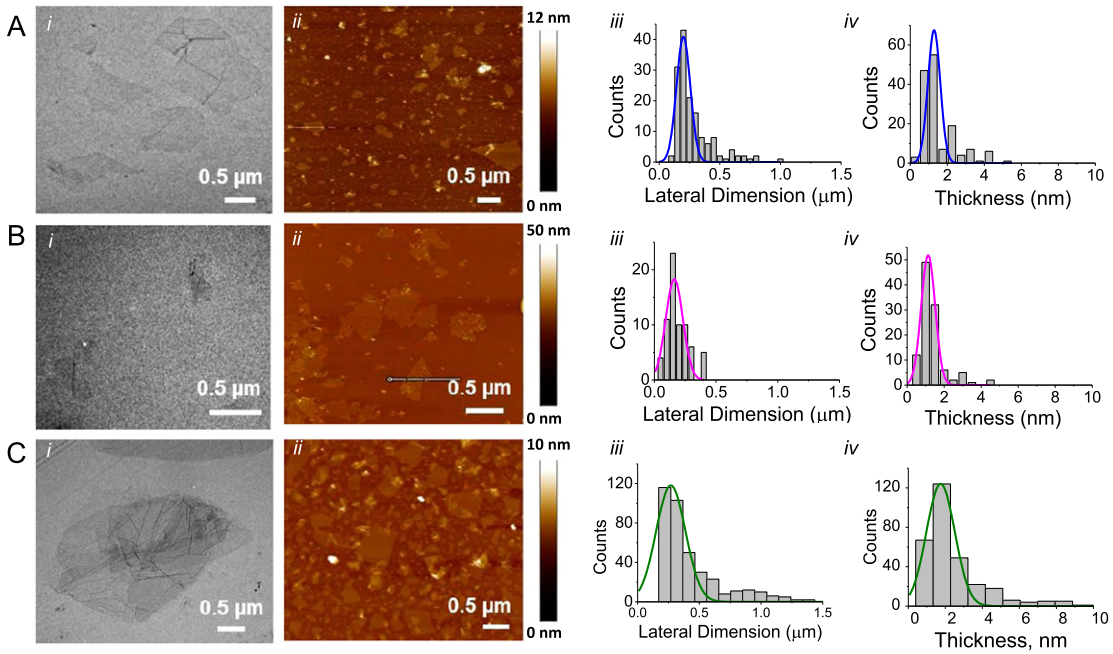

Figure 1. Structural characterisation of (A) GO-f; (B) GO-g; and (C) GO-p. TEM analysis (i); AFM height imaging (ii); lateral size distribution (iii); and thickness distribution (iv). The analysis in (iii) and (iv) was based on counting approximately 100 sheets captured in several AFM images.

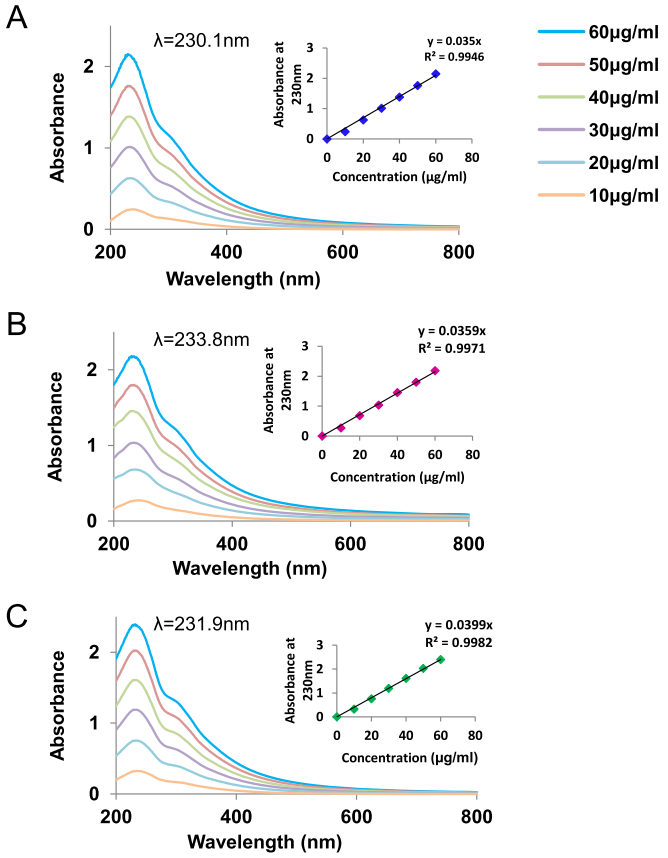

Figure 2. UV/visible spectra of (A) GO-f; (B) GO-g; and (C) GO-p at the concentrations ranging between 10 and 60 μg ml^{-1}. Inset graphs show the absorbance calibration curves at the maximum wavelength.

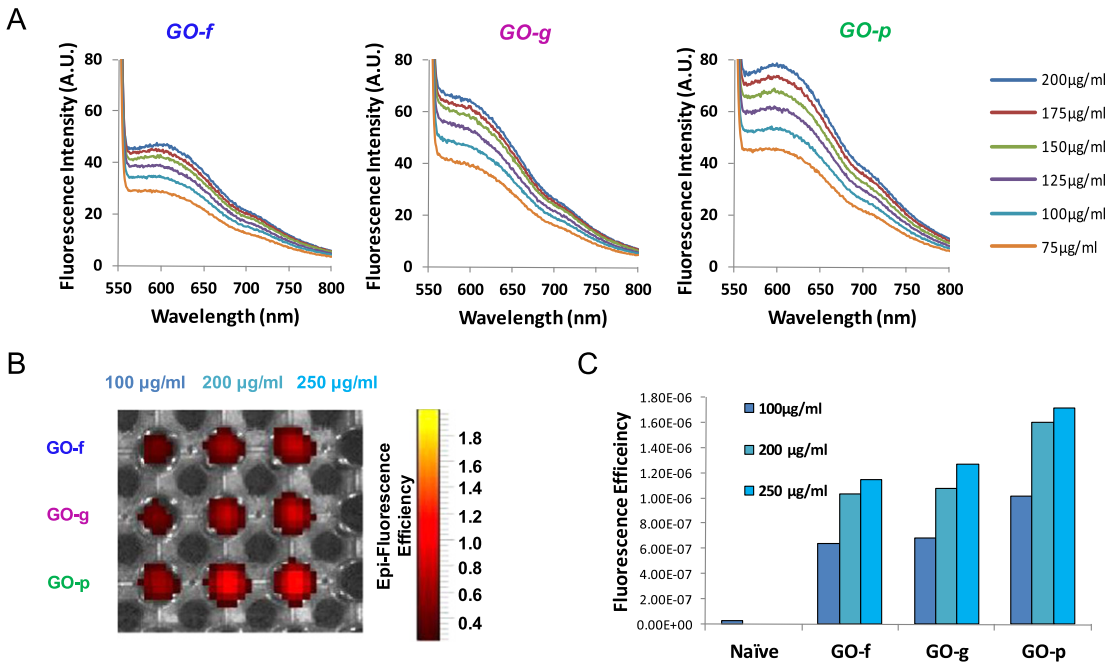

Figure 3. (A) Fluorescence emission spectra at the excitation wavelength of 525 nm of GO-f, GO-g and GO-p at the concentrations ranged from 75 to 200 μg ml^{-1}. (B) IVIS imaging of GO-f, GO-g and GO-p suspensions at 100, 200 and 250 μg ml^{-1}; and (C) the corresponding fluorescence semi-quantification.

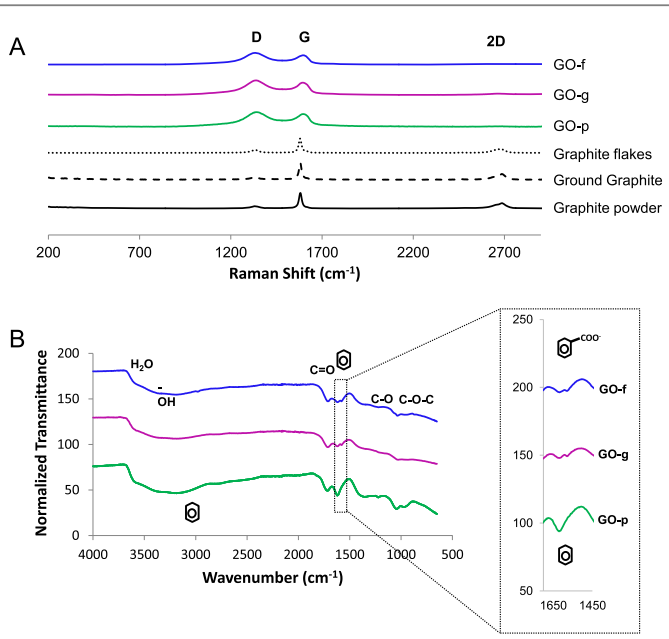

Figure 4. (A) Raman spectra of GO samples prepared from different graphite sources compared to their equivalent starting graphite with corresponding I_D/I_G ratios. (B) Surface functionalities onto GO samples as detected by FT-IR measurements, the magnified image on the right shows the differences detected between samples in the aromatic region (1500–1650 cm^{-1}).

Surface characterisation

Raman scattering of the GO samples prepared were compared to the starting graphite materials after excitation by the visible wavelength (633 nm). All samples had the characteristic G and D bands of most poly-aromatic hydrocarbons [44–47], as shown in figure 4(A). The G band, due to bond-stretching of sp^2 hybridised carbon atoms [45] was present around 1590 cm^{-1} in all samples. This band appeared wider and slightly blue shifted in the GO samples. The disorder D band [46–48] around 1330 cm^{-1} was much more distinct in the GO samples, while the 2D band near 2700 cm^{-1} disappeared, compared to the starting graphite. The D to G band intensity ratio (I_D/I_G),

Table 2. Quantification of degree of functionalisation and functional groups on GO sheets compared to their equivalent starting graphite material using different key metrics. Values are mean ± SD (n = 2–3).

Sample	I_D/I_G	Surface charge (mV)	TGA (% weight loss at 250 °C)	TGA (% weight loss at 550 °C)	Total TGA % weight loss	Titration values COO^- (mmol g^{-1})	XPS % O 1s
GO-f	1.19 ± 0.04	−66.8 ± 2.4	26.3 ± 3.5	17.9 ± 2.8	44.2 ± 0.7	5.2 ± 1.4	27.2 ± 0.7
GO-g	1.21 ± 0.03	−68.6 ± 1.8	22.3 ± 0.8	17.0 ± 1.3	39.6 ± 0.6	4.4 ± 1.0	28.7 ± 2.7
GO-p	1.13 ± 0.04	−61.9 ± 1.8	21.1 ± 2.1	16.1 ± 1.6	37.1 ± 3.0	3.2 ± 0.1	28.6 ± 1.4
Graphite flakes	0.13 ± 0.04	—	0.5 ± 0.3	1.3 ± 0.6	1.8 ± 0.8	—	4.8 ± 0.3
Ground graphite	0.13 ± 0.02	—	0.4 ± 0.2	0.9 ± 0.1	1.3 ± 0.1	—	5.3 ± 1.2
Graphite powder	0.19 ± 0.02	—	0.4 ± 0.4	1.0 ± 0.8	1.3 ± 1.1	—	1.4 ± 0.5

corresponding to the metric of disorder [45, 48] in the graphitic structure is shown in table 2. The I_D/I_G ratio was highest for GO-g. The evolution of Raman bands during the preparation process (figure A1) shows an increase of I_D/I_G ratio gradually as the GO is formed.

Surface charge of the GO samples was determined by ζ-potential measurements using surface charge electrophoresis (Zetasizer NanoZS, Malvern) shown in figure A2 and table 2. GO samples were all highly negatively charged, ranging from −61.9 to −68.6 mV. The instrument software automatically calculates such ζ-potential values using the Henry equation that assumes spherical shape particles. Since GO sheets are non-spherical objects caution is advised in use of the exact ζ-potential values [49].

Identification of surface functional groups

The Fourier transform infrared spectroscopy (FT-IR) was used to identify the functional groups on the surface of GO. Spectra for all GO materials studied are shown in figure 4(B). The oxidation of graphite by our method resulted in the formation of hydroxyl, carboxyl and epoxide groups with the presence of large aromatic regions. However FT-IR cannot give quantification of the oxidation moieties, thus the methods below were used for quantification.

Quantification of functionalisation and purity

Quantification of the surface functional groups was carried out by themo-gravimetric analysis (TGA), x-ray photoelectron spectroscopy (XPS) and conductometric titration. Figure 5(i) displays the TGA curves for the GO products, whereas TGA curves of the starting graphite material are shown in figure A3(i). For all three GO samples studied, two main weight loss steps were observed after subtracting around 10% of evaporated water from 25 °C to 100 °C. Percentage of weight loss of both steps for all samples are shown in table 2.

Conductometric titration was used to quantify the carboxylic groups on GO surfaces [38, 50] as shown in figure A4 and values are listed in table 2. It was not possible to measure the values of the starting graphite material with this method, because of their poor aqueous solubility. Therefore, two different samples of polystyrene beads (carboxylated and non-functionalised polystyrene beads) were used as reference nanomaterials. Carboxylated polystyrene beads had 3.0 ± 1.0 mmol g^{-1} of carboxylic groups, while pristine polystyrene beads showed no inflection in the curve confirming no surface oxidation.

Chemical contamination, C:O ratio and quantification of functional groups present on the GO materials was measured by XPS (figures 5(ii), (iii) and A5 and table 3 and A1). The chemical contamination of GO-f, GO-g and GO-p was 1.6%, 2.3% and 0.4%, respectively, detected from the XPS survey spectra. Contamination for the starting graphite forms was 1.4%, 1.5% and 0% for the flakes, ground and powder material, respectively. The contribution of each chemical element is shown in table A1. The C:O ratio obtained from the XPS survey spectra was 2.6 ± 0.1, 2.4 ± 0.4, 2.5 ± 0.2 for GO-f, GO-g and GO-p respectively. Figure 5(Aiii), (Biii) and (Ciii), show the high resolution C1s XPS spectra for the GO materials. Five components have been fitted for the GO experimental signals (squares) with Gaussian peaks centred at 284.6, 286.6, 287.1, 288.5 and 290.5 eV corresponding to C–C and C=C, C–O–C, C=O, O-C=O and π–π^*, respectively. While only three components were fitted for the starting materials at 284.6, 285.3 and 290.0 eV corresponding to C–C and C=C, C-OH and π–π^*, respectively (figure A3(iii)). Minor (0.1–1 eV) shifts/error in the binding energies were detected between the different GO samples and between different batches for each component (figure A5(E)). The contribution of each individual functional group is shown in table 3. The sp^3 and sp^2 carbon contributions (C–C and C=C) for the GO materials studied, were almost the same for all GO samples (approximately 45%) with higher contributions detected for the starting material (figures A5(A) and (B)). Moderate differences were detected in the percentage of different functional groups as seen in table 3 and figure A5(D). The epoxide contribution was lower for GO-f compared to the GO-g and GO-p, while the carbonyl contribution higher. On the other hand, the carboxylic contribution in GO-g was lower compared to GO-f and GO-p. Some variation between batches of the same material were observed, however no statistical significance was detected between the GOs prepared from different graphite formats (figures A5(B) and (D)). All starting materials exhibited no significant differences in contribution of functional groups (figure A5(C)). Hydroxyl groups were only detected in the starting graphitic material, but not in the GO samples (figures A5(C) and (D)). This could be due to the full oxidation of these oxidation-prone groups or the inability of the fitting used to resolve this peak. The methods used for quantifying the functional groups throughout this work were compared to other techniques such as the Raman I_D/I_G ratio and electrophoretic surface charge in table 2.

Effects of GO exposure on human lung cell cultures

Human lung epithelial cells (A549) where incubated with the different GO samples at escalating concentrations, ranging from 8 to 125 $\mu g\,ml^{-1}$. The dose escalation is based on previous work by our group and others that identified this range as indicative of cytotoxic responses [24]. Cells were viable and replicating at the concentrations studied up to 48 h compared to DMSO 10% treated cells (positive control) that showed significant cytotoxicity. Two cytotoxicity assays (the modified lactate dehydrogenase (LDH) assay and the Trypan blue staining) were

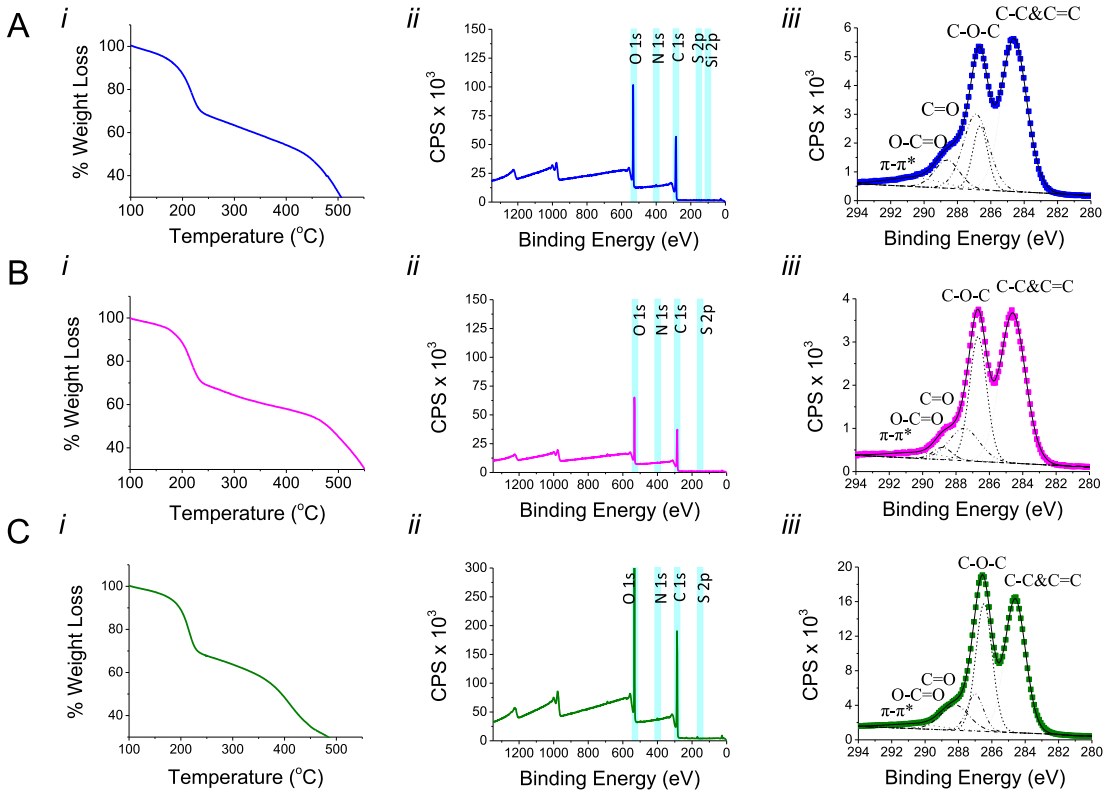

Figure 5. Degree of surface functionalisation for (A) GO-f; (B) GO-g; and (C) GO-p; by TGA (i); chemical contamination by XPS survey spectra (ii); and quantification of functional groups by high resolution C1s XPS spectra (iii).

Table 3. Quantification of π–π^*, carboxylic groups (O–C=O), carbonyls (C=O), epoxides (C–O–C), hydroxyls (C–OH) and graphitic structure (C–C and C=C) by high resolution C 1s XPS spectra for GO-f, GO-g and GO-p. Values are mean ± SD (n = 2–3).

Sample	% π–π^*	% O–C=O	% C=O	% C–O–C	% –OH	% C–C and C=C
GO-f	5.4 ± 1.4	9.5 ± 3.3	22 ± 6.7	19.0 ± 6.4	—	44.1 ± 3.8
GO-g	3.2 ± 1.1	5.6 ± 2.6	15.1 ± 3.5	31.5 ± 4.6	—	44.5 ± 7.3
GO-p	3.9 ± 0.6	8.2 ± 2.8	13.9 ± 4.9	30.0 ± 4.1	—	43.9 ± 0.7

used to cross-validate the findings and eliminate assay-based errors. In general, caution should be exercised in the selection of the cytotoxic assay used in order to avoid optical interference from the carbon material as in the case of MTT (data not shown). Both cytotoxicity assays performed (modified LDH and Trypan blue) indicated no significant cytotoxic responses for all GO samples at the concentrations studied after 24 h and 48 h exposure times (figure 6).

Discussion

We can confirm that the production of few-layered, high-purity GO sheets by using the modified Hummers method was highly reproducible for all three GO samples prepared from flakes, ground and powder graphite. The yields obtained here are lower than those reported by other labs [12, 23] intentionally, in order to extract higher quality and a neutral GO with pH ~ 6.5. The GO gel-like layer (scheme 1) is composed of a high concentration of the very thin and well-dispersed GO, called by Rourke *et al* 'the real GO' [9]. The yield obtained for the GO prepared from the graphite powder (GO-p) was twice as much as the GOs prepared either from the flakes (GO-f) and the ground graphite (GO-g).

One difference detected between the GO samples prepared from different starting graphite forms was the lateral dimension. GO-p exhibited the broadest distribution (containing a small fraction of sheets <1.5 μm), while the other two GO samples, from GO-f and GO-g, produced sheets that were predominantly <500 nm. Size and thickness distributions of GO samples have been reported by previous studies vary significantly, with lateral dimensions ranging from a few nanometres to hundreds of micrometres [8, 51, 52]. Size control is not well-established when using exfoliation top-down synthesis methods for both pristine graphene and GO. Many laboratories are investigating better ways to control size and decrease graphene sheet polydispersity by sonication,

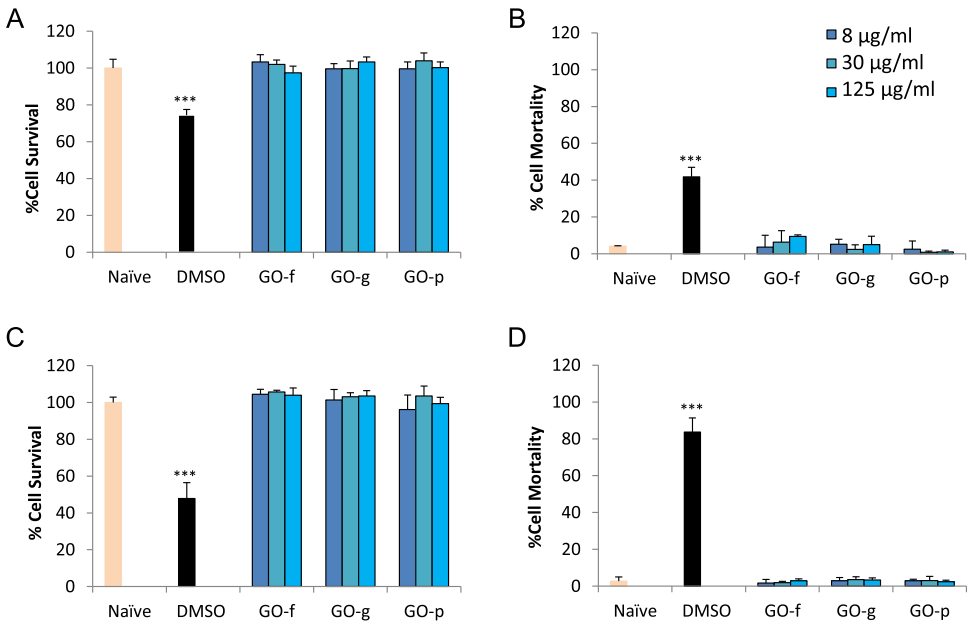

Figure 6. Effect of GO samples on A549 lung carcinoma epithelial cells at 8, 30 and 125 μg ml^{-1} compared to naïve (negative control) and DMSO 10% (positive control) treated cells, tested by the modified LDH assay for (A) 24 h and (C) 48 h; and by Trypan blue cell exclusion assay for (B) 24 h and (D) 48 h. All data are (mean $\pm$ SD) and statistical significance was tested using one way ANOVA with Tukey's post-hoc test ($p < 000.5$ *** against control).

shaking, ultracentrifugation and size separation chromatography [16–18, 52, 53], however all of these processes will bear a structural impact on the final sheets .

The GO sheets obtained here were 1–4 nm in thickness irrespective of the starting graphite. Individual GO sheets have been reported to have a thickness of ~1 nm by AFM and are expected to be 'thicker' than pristine graphene sheets (theoretical thickness of 0.4 nm) [54], due to the presence of the oxidation groups and adsorbed water on the surface [8]. Graphene sheets that have up to 10 single layers can still be considered graphene materials, while thicker flakes should be considered as ultrafine graphite [54, 55]. Our findings suggest that the starting graphite plays an important role in determining the lateral dimensions of the GO sheets, as well as the yield of the GO while the synthetic methodology (oxidation and purification) is the main determinant of the thickness and purity of the GO.

Graphene and its derivatives have specific optical properties, such as UV/visible absorbance and interesting fluorescence properties which can be useful for biological imaging and sensing applications [56]. The absorbance peaks arise from the delocalisation of the π-electrons due to the oxidation process. The 230 nm peak is due to C–C transitions, while that at 300 nm is due to C=O transitions [24, 47, 57]. The fluorescence excitation and emission wavelengths were reproducible for all starting graphite material and for several batches. This indicated that the oxidation method was the determinant factor for the wavelength of emission and excitation rather than the starting material. However, GO-p had the most intense and prominent emission peak among the three GO preparations. Other studies have also shown a similar emission around 600 nm upon different excitation wavelengths in the visible region [52, 57, 58]. It has been shown that the size of the sp^2 clusters within the sp^3 matrix determines the local energy gap and therefore the wavelength of emission. The emissions in the UV–visible region result from sp^2 cluster sizes <1 nm (~20 aromatic rings) and those >2 nm have smaller energy gaps and may account for red-to-NIR emission [8]. The method of GO preparation seems to determine the type of oxidation groups, and therefore act as the critical factor of the optical properties (fluorescence excitation and emission wavelengths). While the larger size of GO-p could relate to the stronger florescence intensity detected, even though fluorescence has been described to originate from the electron transitions between the non-oxidised carbon regions and the oxidised carbon atoms [8, 52, 56–60].

The Raman I_D/I_G ratio increase is generally seen when the degree of disorder by creation of sp^3 bonds is increased [44, 47, 48, 61]. The differences in the I_D/I_G ratio between GO samples prepared from different graphite forms could be related to the differences in the conformation of the carbon atoms at the edges of the starting graphite material [48]. The evolution of Raman bands during the preparation process (shown by the increase of I_D/I_G ratio) was due to the increase in the defects created during the oxidation and exfoliation process and validated the formation of GO sheets for all three different types of graphite.

The resulting GO aqueous dispersions were highly negative, due to the ample surface oxygen

groups. These groups on the GO surface (hydroxyls, epoxides and carbonyls) have been previously identified for material prepared by other methodologies [23, 47, 52, 62, 63]. All three GO samples in this work showed a broad band around (3100–3600 cm^{-1}) due to the associated O–H stretching vibrations, an intense peak at 1730 cm^{-1} for the C=O stretching vibrations and an intense peak at 1070 cm^{-1} for the C–O–C epoxy symmetric stretching vibration [24, 47, 52, 62–66]. In the aromatic region (1500–1650 cm^{-1}) [63, 65] GO-f and GO-g showed two bands around 1590 cm^{-1} and 1640 cm^{-1}. The former could be due to double bonds with one substitution, while the latter is due to aromatic rings with a carboxyl substitution [65, 66]. GO-p had one very intense peak around 1630 cm^{-1}, that was thought to indicate aromatic rings with no substitutions [66]. The difference in the aromatic region between the GO-p and the other two GO samples was the main finding from this FT-IR investigation, and may be related to different substitutions on the aromatic rings based on the configuration of the carbon atoms of the starting material. The broad band around 3000–3100 cm^{-1} was also detected in all GO samples and is indicative of aromatic and unsaturated bonds.

The first mass loss in the TGA curves between 100 °C and 260 °C was thought to be due to the decomposition of the labile oxygen groups (such as carboxylic and aldehydes groups) and the removal of residual water. The second weight loss occurs between 260 °C and 460 °C and is due to the pyrolysis of stable oxygen groups (mainly epoxides) [67, 68]. High-resolution C1s XPS spectra for the GO materials demonstrated successful oxidation with the appearance of higher binding energy contributions (C–O–C, C=O, O–C=O and π–π^*) already reported before [57, 69]. The C:O content appeared to be consistent for all GO samples, however, some differences in the percentage of each functional group were detected depending on the starting graphite form used.

The functionalisation degree for all three GO samples prepared by using both TGA and XPS was found similar, however GO-f showed higher surface carbonyl and carboxyl contributions compared to GO-g and GO-p, observed by both TGA (first weight loss), XPS C1s high-resolution spectra and surface COO^- titration. This could be explained by defects on the π-structure of the graphite flake material that could serve as seed points for the oxidation process [19] or by different carbon atom conformations related to the starting material. On the other hand, GO-g had less carbonyl and carboxylic groups with a slightly more defective surface as seen by the higher I_D/I_G ratio.

Exposure to human lung epithelial cell cultures indicated no differences in biological response to the different GO materials, with no impact on cell viability up to 48 h. Reassuringly, low or no significant cytotoxicity has been reported with GO materials by others [40, 41, 70]. However, other studies have also reported damaging effects on cells by exposure to graphene nanosheets and nanoplatelets, i.e. significantly larger and more inhomogeneous material [71, 72] and GO [73–75]. This variability in the current literature is thought to be related to the many different forms of graphene materials that can result in dramatically different biological outcomes [33]. Much more systematic work is imperative using well characterised GO materials, under accurately defined exposure conditions and biological models before a firm conclusion is reached on the safety of the exposure levels to GO sheets of certain surface and size.

In this work, thin, high-purity (98% to 99%), few-layered GO sheets for biological studies have been synthesised according to a modification of the Hummers method from three different forms of graphite. From the several characterisation techniques performed throughout this work, the main differences identified were in terms of their structural characteristics compared to minute differences among their surface properties. This study indicated that the starting form of graphite can play a determinant role in both the overall yield (with the GO prepared from graphite powder having almost double the yield compared to GO prepared from both graphite flakes and ground graphite) and the lateral dimensions of the ensuing GO sheets for the same synthetic and processing route. Such highly purified, thin and small (<1 μm) GO sheets of physiological pH can be well-tolerated by human lung epithelial cells and were considered encouraging for further development and investigation using more complex biological models and assays.

Experimental

Chemical synthesis of graphene oxide

Three different types of graphite (Chinese flake graphite (Branwell), ground graphite (Branwell), graphite powder (Sigma-Aldrich) were used as the starting material to prepare graphene oxide (GO-f, GO-g and GO-p, respectively), by the modified Hummers method [24]. Briefly, 0.4 g of graphite was mixed with 0.2 g of sodium nitrate ($NaNO_3$) in a beaker, and then 9.2 ml of 96% sulphuric acid (H_2SO_4) was added slowly to the mixture, which was continuously stirred with a magnetic stirrer. The temperature was monitored not to exceed 20 °C by using an ice bath. After obtaining a homogenised mixture, 1.2 g of potassium permanganate ($KMnO_4$) was added slowly. The temperature was monitored again and did not exceed 20 °C. Then the mixture was removed from the ice bath and the temperature started to rise gradually. This was maintained for 30 min until the mixture started thickening and became a paste of dark brown/green colour. Deionized H_2O was added slowly while stirring at the same time. Violent effervescence and rapid increase of temperature was observed. Temperature was monitored carefully and was kept between 98 °C

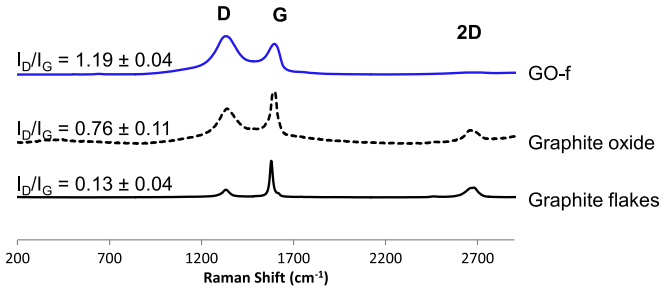

Figure A1. The evolution of the Raman spectrum during the preparation of GO-f by our modified Hummers' method.

and 100 °C for another 30 min with the aid of a hot plate. The mixture was further diluted with 50 ml of deionized H_2O and 3% hydrogen peroxide (H_2O_2) was added gradually for the reduction of the residual KMnO4, manganese dioxide (MnO_2) and manganese heptoxide (Mn_2O_7) to soluble manganese sulphate ($MnSO_4$) salts. The resulting suspension was centrifuged at 8965 rpm for 20 min and the supernatant was discarded, this was repeated until the supernatant had a pH of around 7 and a viscous orange/brown layer of pure GO appeared on top of the oxidation by products. This layer was then separated carefully using warm water; this step should be done carefully to avoid remixing of this layer with the sediment. To determine the concentration of GO a known volume was dried in a glass vial at 50 °C for 24 h. The residue was then placed in a vacuum desiccator for another 24 h in order to remove any remaining humidity and then weighed to determine the final concentration.

Transmission electron microscopy

TEM was performed using a BioTwin electron microscope (Philips/FEI), Tecnai 12 instrument operated at 120 kV accelerating voltage. One drop of sample was placed on a formvar/carbon coated copper grid. Filter paper was used to remove the excess of material.

Atomic force microscopy

A multimode AFM was used on the tapping-mode with an E-type scanner, Nanoscope VI controller, Nanoscope v614r1 control software (Veeco, Cambridge, UK) and a silicon tapping tip (NSG01, NTI-Europe, Apeldoorn, The Netherlands) of 10 nm curvature radius, mounted on a tapping mode silicon cantilever with a typical resonance frequency 150 kHz and a force 14 constant of 5.5 N m^{-1}. Images were taken in air, by depositing 20 μl of the graphene dispersion on a freshly cleaved mica surface (Agar Scientific, Essex, UK) coated with poly-L-Lysine 0.01% (Sigma-Aldrich) and allowed to adsorb for 30 s. Excess unbound material was removed by washing with filtered distilled water, and then allowed to dry in air this step was repeated once. Size and thickness distributions were carried out using ImageJ software, after counting the lateral dimension and height

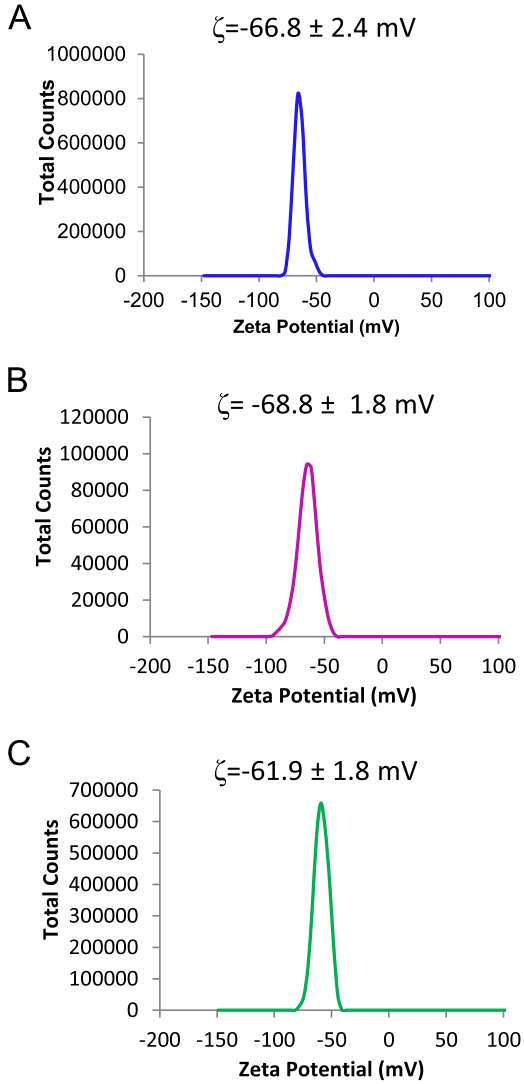

Figure A2. Surface charge data for (A) GO-f; (B) GO-g; and (C) GO-p, expressed as ζ-potential values obtained with the Zetasizer NS (Malvern). Values are mean ± SD; $n = 3$.

respectively of approximately 100 individual graphene sheets, from several AFM images.

UV/visible spectroscopy

UV/visible absorbance spectrum of all samples was measured by a Varian Cary winUV 50 Bio

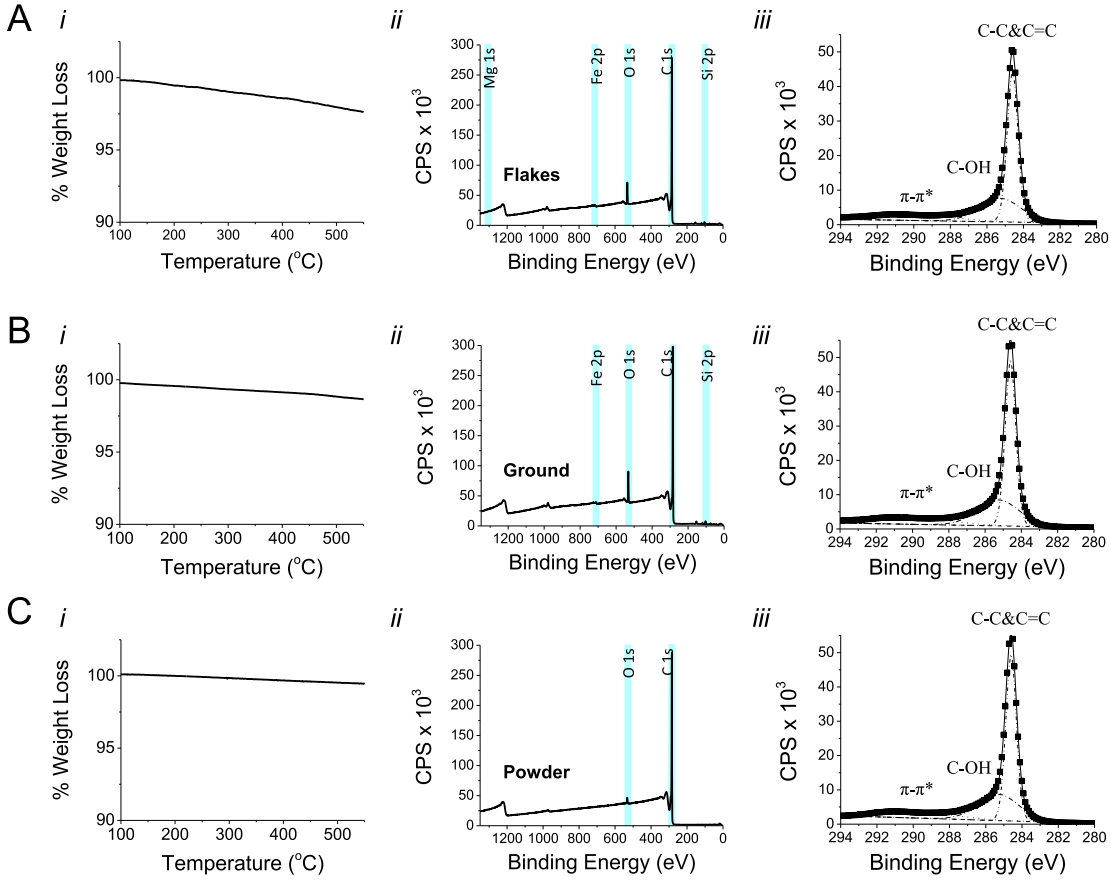

Figure A3. Functionalisation degree of the starting graphite material (A) graphite flakes; (B) ground graphite; and (C) graphite powder by TGA (i); chemical contamination by XPS survey spectra (ii); and quantification of functional groups by high resolution C1s XPS spectra (iii).

spectrophotometer, USA. Samples were diluted ten times in water prior to measurement in a 1 ml glass cuvette with 1 cm path length. Dual beam mode and baseline correction were used throughout the measurements to scan the peak wavelength and maximum absorbance between 200 and 800 nm.

Fluorescence spectroscopy

Fluorescence emission spectra were measured for GO samples at different concentrations (75–200 μg ml^{-1}) using a LS-50B fluorometer (PerkinElmer) at room temperature, with both excitation and emission slits set at 20 nm. The excitation wavelengths used were 483 nm and 525 nm, however 525 nm excitation was only considered as it gave maximum and more linear emission spectra. Fluorochrome absorption was also visualised *in vitro* using an IVIS Lumia II (*in vivo* imaging system), (Caliper Life Sciences Corp., Alameda, CA) using quartz well plates. Three different concentrations of GO samples were tested (100, 200, 250 μg ml^{-1}). Images were displayed as fluorescent efficiency images, where the value of each pixel represents the fractional ratio of fluorescent photons emitted per incident excitation photons. Image acquisitions were performed using the following settings; auto exposure time, binning medium, F stop 2, FOV D, height 1.5, excitation and emission filter of 465, GFP and 535, DsRed for background and original images, respectively. Images were then analysed using Living Image software 3.2 (Caliper Life Sciences Corp).

Raman spectroscopy

Raman Spectra of all samples were recorded after preparing the aqueous dispersions and drop casting them on glass slides and evaporating the solvent. Measurements were carried out using a 50x objective at 633 nm laser excitation using a Renishaw micro-Raman spectrometer. An average of at least three different locations within each sample was measured and 2 to 3 different batches were used to count the I_D/I_G ratio.

Zeta Potential measurements

Electrophoretic mobility (μ) was measured by Malvern Zetasizer Nano ZS (UK) after dilution of samples with water in disposable Zetasizer cuvettes (Malvern Instruments). Default instrument settings and automatic analysis were used for all measurements, where the μ was converted automatically by the equipment software to zeta potential (ζ) values as it is directly related to zeta potential by Henry's equation [76, 77]. All values for samples prepared are triplicate measurements, values were mean $\pm$ SD.

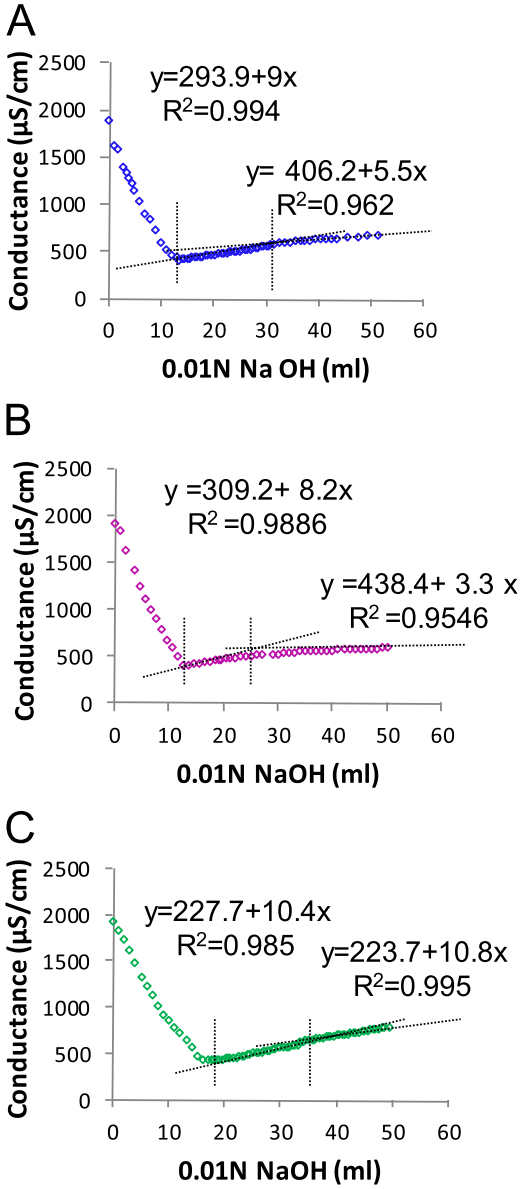

Figure A4. Quantification of the carboxylic groups by conductometric titration of (A) GO-f; (B) GO-g; and (C) GO-p.

Fourier transform infrared spectroscopy

Spectroscopy at the mid-infrared range was carried out on dry samples using a PerkinElmer Spectrum 100 spectrophotometer and the transmittance results were analysed with the built-in spectrum software.

Thermal gravimetric analysis

TGA using a Pyris 6, Perkin-Elmer Ltd was used from 25 °C to 800 °C at 10 °C min^{-1}. Samples (1 to 2 mg) were weighed into a ceramic crucible. Nitrogen (20 ml min^{-1}) was used as a purge gas.

Conductometric titrations

Conductometric titration was used for detection of surface carboxylic group concentrations as described in [38, 50]. In brief, a total quantity of 2 mg of GO was diluted with distilled water. pH of sample was adjusted to 2.5 by 0.01N H_2SO_4 and direct titration with 0.01N NaOH was performed with continuous measurements of conductance by a Primo5 conductometer (HANNA Instruments, UK) and pH with a pH-meter upon addition of equal increments of NaOH with continuous stirring and allowing 1 min of stabilisation after each addition. Volumes were recorded until pH 11 and the surface carboxyl intensity (mmol g^{-1}) was calculated by the following equation:

$$\text{Carboxylic groups intensity (mmol g}^{-1}) = 10^3 \times M(V2 - V1)/W,$$

where M (mol l^{-1}) is the concentration of NaOH, $(V2 - V1)$ (ml) is the linear fitting volume of NaOH, and W(g) is the GO quality.

X-ray photoelectron spectroscopy

The composition of GO surfaces was studied by XPS at NEXUS facility (the UK's National EPSRC XPS Users' Service, hosted by nanoLAB in Newcastle-upon-Tyne). XPS was recorded using a Thermo Theta Probe XPS spectrometer with a monochromatic Al K-α source of 1486.68 eV. The survey XPS spectra were acquired with pass energy (PE) of 200 eV, 1 eV step size, 50 ms dwell time and averaged over 5 scans. The etching was 90 s. The high resolution C1s XPS spectra were acquired with PE of 40 eV, 0.1 eV step size, 100 ms dwell time and averaged over 20 scans. Spectra from insulating samples have been charge corrected by shifting all peaks to the adventitious carbon C 1s spectral component binding energy set to 284.6 eV. *CasaXPS* software has been used to process the spectra acquired at NEXUS.

Cell cultures

Culture of A549 monolayers (epithelial lung carcinoma cells (A549; ATCC, CCL-185)) were maintained and passaged in F12 Ham media supplemented with 10% FBS, 50 U ml^{-1} penicillin, at 37 °C in 5% CO_2. Cells were passaged twice a week using trypsin-EDTA 0.05% when reaching 80% confluence. Cellular interaction of GO with A549 cells, were predicted by seeding A549 cells into 96-well plates (10 000 cells/well) or 6-well plates (100 000 cells per well) depending on the assay as described below and left to attach overnight before incubation with GO sterile solutions in 5% dextrose. Cells were then incubated from 1–48 h with GO-f, GO-g and GO-p (0–125 μg ml^{-1}) in complete media at 37 °C in a humidified atmosphere (5% CO_2). For sterilisation and limiting contamination samples were dried in oven at 50 °C and desiccated overnight, then reconstituted to the desired concentrations in sterile dextrose 5% prior to use on cells.

Modified LDH assay

A modified LDH assay was used as described in [78], to avoid any interference related to the auto-fluorescence

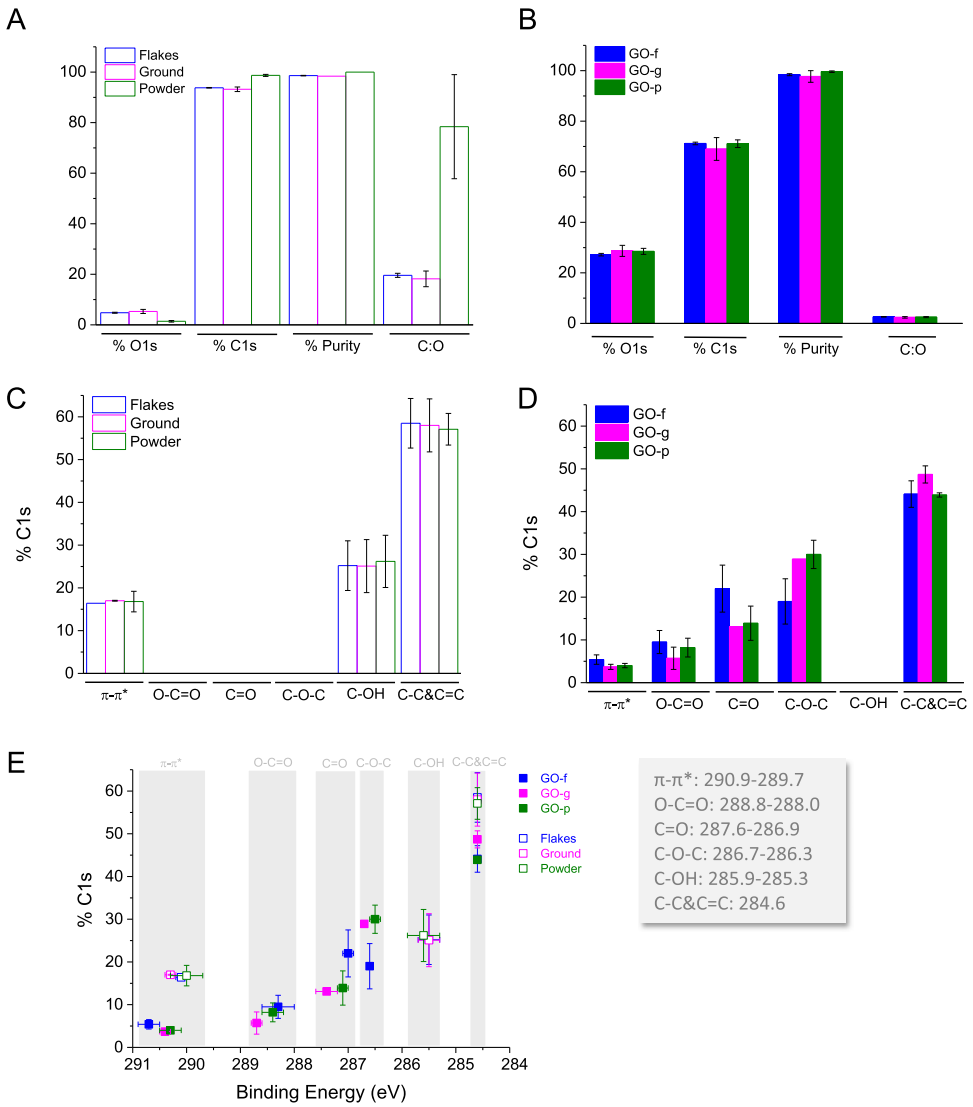

Figure A5. % O1s, % C1s, % purity and C:O ratio for: (A) the different sources of graphitic material (flakes, ground and powder graphite) and for (B) the corresponding GOs (GO-f, GO-g and GO-p). % C1s contributions (π–π^*, O–C=O, C=O, C–O–C, C–OH and C–C and C=C) for (C) the different sources of graphite and (D) the corresponding GOs. (E) Summary of the % C1s and binding energies for each individual C1s contribution of graphite and GOs. Data are mean ± SD and no statistical significance was observed using one way ANOVA with Tukey's post-hoc test.

of GO itself. The LDH leakage was assessed in the survived cells, rather than the LDH released in the media upon GO induced-cell death. Therefore, the media containing dead cells was aspirated and the intact cells were lysed with 10 μl of lysis buffer (0.9% Triton X100) mixed with 100 μl serum and phenol free media, for 45–60 min at 37 °C to obtain a cell lysate which was then centrifuged at 16060 xg for 5 min in order to pellet down the GO. Fifty microliters of the supernatant of the cell lysate was mixed with 50 μl of LDH substrate mix in a new microtiter plate and incubated for 15 min at room temperature. Absorbance was read at 490 nm using a plate reader. The amount of LDH detected represented the number of live cells which survived the treatment. The percentage cell survival was calculated using the following equation:

$$\text{Percentage cell survival} = A_{490\,\text{nm}} \text{ of treated cells} / A_{490\,\text{nm}} \text{ of untreated cells} \times 100.$$

Trypan blue cell exclusion assay

Trypan blue assay was carried out to determine the cell mortality. A549 cells were plated in 6-well plates (100 000 cells per well) and left to adhere overnight. The cells were then incubated with GO at different concentrations (0–125 μg ml^{-1}) in complete media. Untreated cells cultured in free medium were taken as the control. Twenty-four and forty-eight hours later, the supernatants was collected and the cells were detached with 300 μl trypsin–EDTA solution. The mixture of the supernatant and detached cells was centrifuged at 1500 rpm for 5 min. Then cells were redispersed in complete media and an equal volume of Trypan blue solution was added. After 5 min staining, cells were counted using cytometer. The dead cells

Table A1. Quantification of Na 1s, Mg 1s, Fe 2p, O 1s, N 1s, C 1s, S 2p and Si 2p regions from the XPS survey spectra of GO-f, GO-g, GO-p, GBM and the different forms of graphite used. C:O ratio and purity calculated from the elemental quantification. Values are mean ± SD (n = 2–3).

Sample	% Na 1s	% Mg 1s	% Fe 2p	% O 1s	% N 1s	% C 1s	% S 2p	% Si 2p	C:O	% Purity
GO-f	—	—	—	27.2 ± 0.7	0.3 ± 0.5	71.2 ± 0.6	1.2 ± 1.0	0.2 ± 0.3	2.6 ± 0.1	98.4 ± 0.6
GO-g	—	—	—	28.7 ± 2.7	0.5 ± 0.6	69.0 ± 5.5	0.5 ± 0.5	1.5 ± 2.7	2.4 ± 0.4	97.7 ± 2.9
GO-p	—	—	—	28.5 ± 1.5	0.1 ± 0.2	71.1 ± 1.8	0.5 ± 0.0	—	2.5 ± 0.2	99.6 ± 0.4
Graphite flakes	—	0.1 ± 0.1	0.1 ± 0.1	4.8 ± 0.3	—	93.9 ± 0.1	—	1.4 ± 0.2	19.6 ± 1.2	98.6 ± 0.1
Ground graphite	—	—	0.1 ± 0.1	5.3 ± 1.2	—	93.2 ± 1.2	—	1.6 ± 0.0	18.3 ± 4.5	98.5 ± 0.1
Graphite powder	—	—	—	1.4 ± 0.5	—	98.7 ± 0.5	—	—	78.4 ± 29.1	100 ± 0.0

were stained in blue. The percentage cell mortality was counted from the following equation:

$$\text{Percentage cell mortality} = \text{Dead cell count}/\text{Total cell count} \times 100.$$

Statistical analysis

All experiments were repeated at least twice and data are represented as mean ± standard deviation (SD). Cellular experiments were carried out in four replicates. Statistical significance was tested using one way ANOVA with Tukey's post-hoc test ($p < 0.005$ ***, $p < 0.01$ ** and $p < 0.05$ *).

Acknowledgments

X-ray photoelectron spectra were obtained at the National EPSRC XPS User's Service (NEXUS) at Newcastle University, an EPSRC Mid-Range Facility. We thank Dr Jose Portoles from NEXUS facility for XPS measurements and assistance. We are also grateful to Dr Nigel Hodson from the AFM facility at the Stopford building in the University of Manchester for assistance and advice with the AFM instrumentation. The authors gratefully acknowledge financial support from EU FP7-ICT-2013-FET-F GRAPHENE Flagship project (no. 604391).

Appendix

References

[1] Novoselov K S *et al* 2005 Two-dimensional atomic crystals *Proc. Natl Acad. Sci. USA* **102** 10451–3
[2] Geim A K 2009 Graphene: status and prospects *Science* **324** 1530–4
[3] Kostarelos K and Novoselov K S 2014 Graphene devices for life *Nat. Nano* **9** 744–5
[4] Bitounis D, Ali-Boucetta H, Hong B H, Min D H and Kostarelos K 2013 Prospects and challenges of graphene in biomedical applications *Adv. Mater.* **25** 2258–68
[5] Pan Y, Sahoo N G and Li L 2012 The application of graphene oxide in drug delivery *Expert Opin. Drug Deliv.* **9** 1365–76
[6] Shen H, Zhang L, Liu M and Zhang Z 2012 Biomedical applications of graphene *Theranostics* **2** 283–94
[7] Chng E L K and Pumera M 2013 The toxicity of graphene oxides: dependence on the oxidative methods used *Chem.—Eur. J.* **19** 8227–35
[8] Loh K P, Bao Q, Eda G and Chhowalla M 2010 Graphene oxide as a chemically tunable platform for optical applications *Nat. Chem.* **2** 1015–24
[9] Rourke J P *et al* 2011 The real graphene oxide revealed: stripping the oxidative debris from the graphene-like sheets *Angew. Chem. Int. Ed.* **50** 3173–7
[10] Kim K S *et al* 2009 Large-scale pattern growth of graphene films for stretchable transparent electrodes *Nature* **457** 706–10
[11] Feng L and Liu Z 2011 Graphene in biomedicine: opportunities and challenges *Nanomedicine* **6** 317–24
[12] Zhu Y, James D K and Tour J M 2012 New routes to graphene, graphene oxide and their related applications *Adv. Mater.* **24** 4924–55
[13] Lotya M, King P J, Khan U, De S and Coleman J N 2010 High-concentration, surfactant-stabilized graphene dispersions *ACS Nano* **4** 3155–62
[14] Park S and Ruoff R S 2009 Chemical methods for the production of graphenes *Nat. Nanotechnology* **4** 217–24
[15] Leon V *et al* 2011 Few-layer graphenes from ball-milling of graphite with melamine *Chem. Commun.* **47** 10936–8
[16] Krane N 2011 Preparation of graphene *Selected Topics in Physics: Physics of the Nanoscale* (Berlin: Freie Univ.)
[17] Smith R J, King P J, Wirtz C, Duesberg G S and Coleman J N 2012 Lateral size selection of surfactant-stabilised graphene flakes using size exclusion chromatography *Chem. Phys. Lett.* **531** 169–72
[18] Sun X, Luo D, Liu J and Evans D G 2010 Monodisperse chemically modified graphene obtained by density gradient ultracentrifugal rate separation *ACS Nano* **4** 3381–9
[19] Dreyer D R, Park S, Bielawski C W and Ruoff R S 2010 The chemistry of graphene oxide *Chem. Soc. Rev.* **39** 228–40
[20] Staudenmaier L 1898 Verfahren zur darstellung der graphitsäure *Ber. Dtsch. Chemischen Ges.* **31** 1481–7
[21] Hofmann U and Holst R 1939 Über die säurenatur und die methylierung von graphitoxyd *Ber. Dtsch. Chemischen Ges.* A and B **72** 754–71
[22] Hummers W S and Offeman R E 1958 Preparation of graphitic oxide *J. Am. Chem. Soc.* **80** 1339–1339
[23] Marcano D C *et al* 2010 Improved synthesis of graphene oxide *ACS Nano* **4** 4806–14
[24] Ali-Boucetta H *et al* 2012 Purified graphene oxide dispersions lack *in vitro* cytotoxicity and *in vivo* pathogenicity *Adv. Healthc. Mater.* **2** 433–41
[25] Kovtyukhova N I *et al* 1999 Layer-by-layer assembly of ultrathin composite films from micron-sized graphite oxide sheets and polycations *Chem. Mater.* **11** 771–8
[26] Richtera L *et al* 2014 The impact of graphite source and the synthesis method on the properties of graphene oxide *Key Eng. Mater.* **592–3** 374–7
[27] Bianco A 2013 Graphene: safe or toxic? the two faces of the medal *Angew. Chem. Int. Ed.* **52** 4986–97
[28] Bussy C, Ali-Boucetta H and Kostarelos K 2012 Safety considerations for graphene: lessons learnt from carbon nanotubes *Acc. Chem. Res.* **46** 692–701
[29] Bussy C, Jasim D A, Lozano N, Terry D and Kostarelos K 2015 The current graphene safety landscape—a literature mining exercise *Nanoscale* **7** 6432–5
[30] Panariti A, Miserocchi G and Rivolta I 2012 The effect of nanoparticle uptake on cellular behavior: disrupting or enabling functions? *Nanotechnology Sci. Appl.* **5** 87–100
[31] Russier J *et al* 2013 Evidencing a mask effect of graphene oxide: a comparative study on primary human and murine phagocytic cells *Nanoscale* **5** 11234–47
[32] Novoselov K S *et al* 2012 A roadmap for graphene *Nature* **490** 192–200
[33] Kostarelos K and Novoselov K S 2014 Exploring the interface of graphene and biology *Science* **344** 261–3
[34] Willi P and Sharma C P 2011 Blood compatibility and biomedical applications of graphene *Trends Biomater. Artif. Organs* **25** 91–4
[35] Ryoo S-R, Kim Y-K, Kim M-H and Min D-H 2010 Behaviors of NIH-3T3 fibroblasts on graphene/carbon nanotubes: proliferation, focal adhesion, and gene transfection studies *ACS Nano* **4** 6587–98
[36] Wang Y *et al* 2012 Fluorinated graphene for promoting neuro-induction of stem cells *Adv. Mater.* **24** 4285–90
[37] Zhang Y *et al* 2010 Cytotoxicity effects of graphene and single-wall carbon nanotubes in neural phaeochromocytoma-derived PC12 cells *ACS Nano* **4** 3181–6
[38] Yue H *et al* 2012 The role of the lateral dimension of graphene oxide in the regulation of cellular responses *Biomaterials* **33** 4013–21
[39] Liao K H, Lin Y S, Macosko C W and Haynes C L 2011 Cytotoxicity of graphene oxide and graphene in human

erythrocytes and skin fibroblasts *ACS Appl. Mater. Interfaces* **3** 2607–15
[40] Sasidharan A *et al* 2012 Differential nano-bio interactions and toxicity effects of pristine versus functionalized graphene *Nanoscale* **3** 2461–4
[41] Sasidharan A *et al* 2012 Hemocompatibility and macrophage response of pristine and functionalized graphene *Small* **8** 1251–63
[42] Agarwal S *et al* 2010 Interfacing live cells with nanocarbon substrates *Langmuir* **26** 2244–7
[43] Hu W *et al* 2010 Graphene-based antibacterial paper *ACS Nano* **4** 4317–23
[44] Casiraghi C *et al* 2009 Raman spectroscopy of graphene edges *Nano Lett.* **9** 1433–41
[45] Ferrari A C 2007 Raman spectroscopy of graphene and graphite: disorder, electron–phonon coupling, doping and non-adiabatic effects *Solid State Commun.* **143** 47–57
[46] Ferrari A C *et al* 2006 Raman spectrum of graphene and graphene layers *Phys. Rev. Lett.* **97** 187401
[47] Rattana *et al* 2012 Preparation and characterization of graphene oxide nanosheets *Proc. Eng.* **32** 759–64
[48] Zhu Y *et al* 2010 Graphene and graphene oxide: synthesis, properties, and applications *Adv. Mater.* **22** 3906–24
[49] Hunter R J 1988 *Zeta Potential In Colloid Science: Principles And Applications* (London: Academic)
[50] Hen J 1974 Determination of surface carbonyl groups in styrene/itaconic acid copolymer latexes *J. Colloid Interface Sci.* **49** 425–32
[51] Eda G and Chhowalla M 2009 Graphene-based composite thin films for electronics *Nano Lett.* **9** 814–8
[52] Sun X *et al* 2008 Nano-graphene oxide for cellular imaging and drug delivery *NanoResearch* **1** 203–12
[53] Wang X, Bai H and Shi G 2011 Size fractionation of graphene oxide sheets by pH-assisted selective sedimentation *J. Am. Chem. Soc.* **133** 6338–42
[54] Geim A K and Novoselov K S 2007 The rise of graphene *Nat. Mater.* **6** 183–91
[55] Wick P *et al* 2014 Classification framework for graphene-based materials *Angew. Chem. Int. Ed.* **23** 7714–8
[56] Qian J *et al* 2012 Observation of multiphoton-induced fluorescence from graphene oxide nanoparticles and applications in *in vivo* functional bioimaging *Angew. Chem. Int. Ed.* **51** 10570–5
[57] Shang J *et al* 2012 The origin of fluorescence from graphene oxide *Sci. Rep.* **2** 792
[58] Galande C *et al* 2011 Quasi-molecular fluorescence from graphene oxide *Sci. Rep.* **1** 85
[59] Eda G *et al* 2010 Blue photoluminescence from chemically derived graphene oxide *Adv. Mater.* **22** 505–9
[60] Thomas H R *et al* 2013 Identifying the fluorescence of graphene oxide *J. Mater. Chem.* C **1** 338–42
[61] Cancado L G *et al* 2006 General equation for the determination of the crystallite size L-a of nanographite by Raman spectroscopy *Appl. Phys. Lett.* **88** 163106
[62] Choi E-Y *et al* 2010 Non-covalent functionalization of graphene with end-functional polymers *J. Mater. Chem.* **20** 1907–12
[63] Wang G *et al* 2009 Synthesis of enhanced hydrophilic and hydrophobic graphene oxide nanosheets by a solvothermal method *Carbon* **47** 68–72
[64] Willard H, Merritt L, Dean J and Settle F 1988 *Instrumental Methods of Analysis* 7th edn (California: Wadsworth, Inc)
[65] Williams D H and Feleming I 1995 *Spectroscopic Methods in Organic Chemistry* 5th edn (England: McGraw-Hill)
[66] Pretsch E, Clerc T, Seibl J and Simon W 1989 *Tables of Spectral Data for Structure Determination of Organic Compounds* (Brooklyn, NY, USA: Springer)
[67] Namvari M and Namazi H 2014 Sweet graphene I: toward hydrophilic graphene nanosheets via click grafting alkyne-saccharides onto azide-functionalized graphene oxide *Carbohydrate Res.* **396** 1–8
[68] Neelgund G M, Oki A and Luo Z 2014 ZnO and cobalt phthalocyanine hybridized graphene: efficient photocatalysts for degradation of rhodamine B *J. Colloid Interface Sci.* **430** 257–64
[69] Liu Z, Duan X, Qian G, Zhou X and Yuan W 2013 Eco-friendly one-pot synthesis of highly dispersible functionalized graphene nanosheets with free amino groups *Nanotechnology* **24** 0957–4484
[70] Chang Y *et al* 2011 *In vitro* toxicity evaluation of graphene oxide on A549 cells *Toxicology Lett.* **200** 201–10
[71] Li Y *et al* 2013 Graphene microsheets enter cells through spontaneous membrane penetration at edge asperities and corner sites *Proc. Natl Acad. Sci.* **110** 12295–300
[72] Tu Y *et al* 2013 Destructive extraction of phospholipids from *Escherichia coli* membranes by graphene nanosheets *Nat. Nanotechnology* **8** 594–601
[73] Lammel T, Boisseaux P, Fernandez-Cruz M-L and Navas J 2013 Internalization and cytotoxicity of graphene oxide and carboxyl graphene nanoplatelets in the human hepatocellular carcinoma cell line Hep G2 *Part. Fibre Toxicology* **10** 27
[74] Akhavan O and Ghaderi E 2010 Toxicity of graphene and graphene oxide nanowalls against bacteria *ACS Nano* **4** 5731–6
[75] Wan B *et al* 2013 Single-walled carbon nanotubes and graphene oxides induce autophagosome accumulation and lysosome impairment in primarily cultured murine peritoneal macrophages *Toxicoloy Lett.* **221** 118–27
[76] Adamson A W 1990 *Physical Chemistry of Surfaces* (New York: Wiley-Interscience)
[77] Lozano N *et al* 2009 Catanionic vesicles formed with arginine-based surfactants and 1,2-dipalmitoyl-sn-glycero-3-phosphate monosodium salt *J. Phys. Chem.* B **113** 6321–7
[78] Ali-Boucetta H *et al* 2011 Cellular uptake and cytotoxic impact of chemically functionalized and polymer-coated carbon nanotubes *Small* **7** 3230–8